

Received 14 February 2022; revised 8 April 2022; accepted 8 April 2022. Date of publication 12 April 2022; date of current version 2 August 2022.
The review of this article was arranged by Editor L. Hutin.

Digital Object Identifier 10.1109/JEDS.2022.3166683

Optimum Functionalization of Si Nanowire FET for Electrical Detection of DNA Hybridization

R. MIDAHUEN¹, B. PREVITALI¹, C. FONTELAYE¹, G. NONGLATON¹, V. STAMBOULI², AND S. BARRAUD¹

¹ CEA, LETI, MINATEC Campus and Univ. Grenoble Alpes, 38054 Grenoble, France
² Univ. Grenoble Alpes, CNRS, Grenoble-INP, LMGP, 38000 Grenoble, France

CORRESPONDING AUTHOR: S. BARRAUD (e-mail: sylvain.barraud@cea.fr)

This work was supported in part by the French Public Authorities through the NANO 2022 Program; in part by the ANR through the LabEx ARCANE Program under Grant ANR-11-LABX-0003-01; and in part by the Graduate School on Chemistry, Biology and Health of Univ. Grenoble Alpes CBH-EUR-GS under Grant ANR-17-EURE-0003.

ABSTRACT In this work, we demonstrate a wafer-scale fabrication of biologically sensitive Si nanowire FET for pH sensing and electrical detection of deoxyribonucleic acid (DNA) hybridization. Based on conventional “top-down” CMOS compatible technology, our bioFETs explore a wide range of design (nanowires (NW), nanoribbons (NR), and honeycomb (HC) structures) with opening access scaled down to only 120 nm. After device fabrication, I_{DS} - V_{BG} transfer and I_{DS} - V_{DS} output characteristics show a conventional n-type FET behavior with an I_{ON}/I_{OFF} value higher than 10^5 , as well as an increase of threshold voltage as the NW width is reduced. Then, using a capacitive coupling in our dually-gated Si bioFETs, the pH sensitivity is enhanced with a pH response up to 600 mV/pH. Finally, we successfully detected an increase of threshold voltage of n-type silicon nanowires (SiNWs) due to hybridized target DNA molecules.

INDEX TERMS Biosensing, ISFET, DNA, silicon nanowire.

I. INTRODUCTION

Massive amount of researches have been devoted to the development of accurate and sensitive portable biosensors for various diagnostic applications ranging from medical diagnosis to environmental monitoring of potentially harmful pollutants. In this context, Ion sensitive field-effect transistors (ISFETs) appear as suitable tools for key biochemical analysis such as real-time and label-free DNA sequencing [1], real-time detection of DNA [2], proteins [3], viruses [4], and gas [5].

The basic ISFET device structure [6] is analogous to Metal–Oxide–Semiconductor Field Effect Transistor (MOSFET). The main dissimilarity relies on the removal of the front metal gate electrode, which is replaced by a sensing site whereby an electrolyte solution can be directly deposited on the device gate oxide. At this electrolyte/gate oxide interface, the phenomenon of pH dependent protonation or deprotonation of the oxide amphoteric groups, or the adsorption of charged molecules over the gate oxide, modifies locally the profile of electrical potential. Charging the gate oxide can significantly modulate

the threshold voltage (V_{TH}) or the drain current (I_{DS}) of the device [7], [8]. Among various types of ISFETs, SiNW-based devices are ones of the most promising due to their small width (below tens of nanometers), their ability to be densely integrated, and their large surface-to-volume ratio with high gate controllability, leading to an improved sensitivity [9], [10].

In this work, we use ISFETs with different designs and geometries such as Si nanowire (NW), nanoribbon (NR) and honeycomb (HC) structures for pH sensing. Thanks to a capacitive coupling of our dually-gated devices, we demonstrate an enhanced pH sensitivity of 600 mV/pH, which is ten times higher than the conventional Nernstian response of 59 mV/pH.

After pH sensing experiments, we implemented an epoxysilane high-quality surface functionalization process that removed the non-idealities encountered with the aminosilane (APTES) functionalization protocol. Finally, regardless of the biofunctionalization protocol employed, we demonstrated label-free electrical detection of targeted DNA molecules.

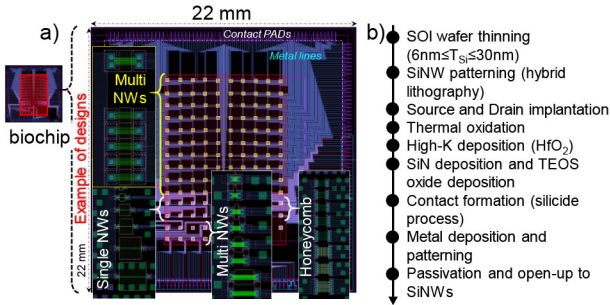


FIGURE 1. (a) Mask set design used for the fabrication of Si bioFETs. The die size is 22 mm × 22 mm. Si nanowire, nanoribbon and honeycomb structures are defined with different dimensions. (b) Main technological steps used in the fabrication of Si bioFETs devices.

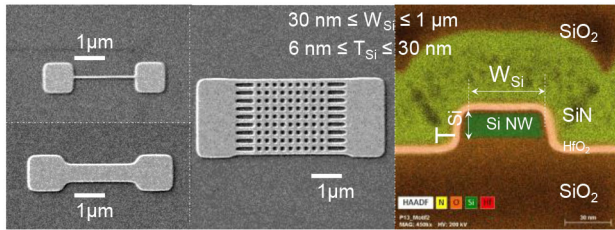


FIGURE 2. Scanning Electron Microscopy (SEM) images and Energy-Dispersive X-ray (EDX) spectroscopy of multiple designs after patterning (nanowire, nanoribbon, and honeycomb structures). The smallest dimension of nanowires after etching is $W=30$ nm.

II. FABRICATION PROCESS

A. LAYOUT AND MAIN TECHNOLOGICAL STEPS

The layout design used for the fabrication of our Si biologically sensitive field-effect transistors (bioFETs) is shown in Fig. 1(a). All the devices are located in the center of the die (inside the red rectangle) enabling a future integration of a microfluidic system which is a cheap and simple method for multiplexed electrical detection of biological or chemical species. The main technological steps used in the fabrication of our Si bioFET are given in Fig. 1b. We start from a (100)-oriented SOI wafer. The Si layer is oxidized to target a Si thickness varying between 6 nm and 30 nm after oxide removal. As shown in Fig. 2, multiples designs are patterned by means of a top-down hybrid deep ultraviolet (DUV) and electron-beam lithography followed by a reactive ion etching. Devices with feature sizes above 300 nm are patterned using DUV lithography, while electron-beam lithography is employed for smaller dimensions. The smallest NW width obtained after etching is 30 nm (Fig. 2).

Once patterned, a lithography step is performed to form the source / drain (S/D) terminals by a phosphorus ion implantation targeting a doping of 10^{20} cm⁻³. Next, a high-quality 3 nm thick SiO₂ layer was thermally grown on the Si surface before the deposition of a 4 nm thick HfO₂ layer. HfO₂ layer is selected as the sensing surface for its excellent pH sensing properties and due to its great chemical stability in most acidic and basic solutions [11]. Then, a silicon nitride (of thickness 50 nm) and Tetraethyl

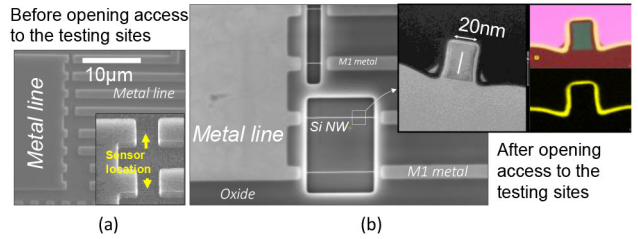


FIGURE 3. (a) Scanning electron microscopy (SEM) images after metal etching. (b) SEM and Transmission electron microscopy (TEM) images after opening access to the sensing site. The etch stop layer is the HfO₂ layer.

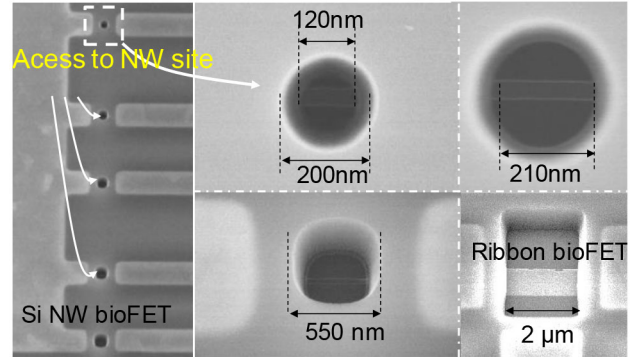


FIGURE 4. SEM images showing ultra-scaled opening access with dimensions down to only 120 nm.

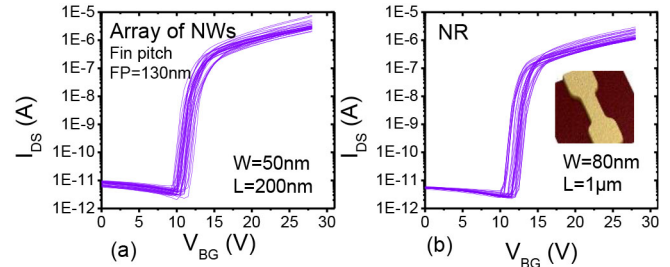


FIGURE 5. I_{DS} - V_{BG} transfer characteristics with $V_{DS} = 1$ V after opening access to (a) SiNWs and (b) SiNRs.

Orthosilicate (TEOS, of thickness 250 nm) layers are deposited. A Chemical Mechanical Polishing (CMP) is performed on TEOS layer before the formation of S/D integrating low resistance ohmic contact (NiSi). Then, we realized a one-level metallization scheme, as shown in Fig. 3(a). Finally, the metal layer is passivated with a 100 nm thick SiO₂ dielectric before using an additional lithography followed by an etching step to open the Si NW/NR/HC sensing site (Fig. 3(b)). As shown in Fig. 4, access opening scaled down to only 120 nm are obtained in order to identify the limit of wettability of the cavities due to their decreasing sizes.

B. DRY ELECTRICAL CHARACTERIZATION

First, we electrically measured our Si bioFETs to be ensured of their integrity. Electrical characterization was conducted on a HP 4155A Analyzer connected to a probe station. The drain current (I_{DS}) vs back-gate voltage (V_{BG}) was measured

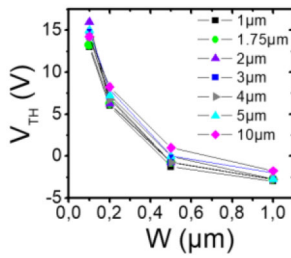


FIGURE 6. Threshold voltage V_{TH} versus W for SiNRs with various channel lengths ($1\mu\text{m} < L < 10\mu\text{m}$).

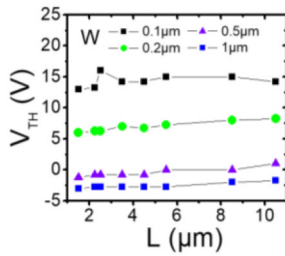


FIGURE 7. Threshold voltage V_{TH} versus L for SiNRs with various widths W ($0.1\mu\text{m} < W < 1\mu\text{m}$).

at $V_{DS} = 1\text{ V}$ for various designs and geometries (SiNW, SiNR, SiHC). Fig. 5 shows representative $I_{DS}-V_{BG}$ transfer characteristics for Si NW arrays and NRs. The devices show typical n -MOSFETs characteristics with an I_{ON}/I_{OFF} ratio higher than 10^5 . The width dependence of threshold voltage (Fig. 6) clearly shows an increase of V_{TH} with the reduction of the NW width. However, as shown in Fig. 7, due to a large enough channel length, we do not observe short-channel effects.

III. ION SENSITIVE FIELD EFFECT TRANSISTORS

Before DNA grafting and electrical detection of hybridization, we first used pH-sensing experiment to study the charge-sensitivity response of our bioFETs.

The pH-sensing measurements were carried out from standard buffer solutions with seven different pH values (i.e., pH 4 to 10). Solutions of Tris (1M) are titrated with HCl to obtain basic pH solutions between 8 and 10. Following the same scheme, solutions of Sodium acetate (100 mM) are titrated with acetic acid to obtain acidic and neutral pH solutions (from pH 4 to pH 7). *First*, our devices operated at $V_{DS} = 1\text{ V}$, $V_{BG} = 15\text{ V}$, while I_{DS} is modulated by an Ag/AgCl reference electrode immersed in the probed pH solution (as schematized in the inset of Fig. 8(b)). We obtained transfer curves by sweeping the pH solution potential with the immersed reference electrode voltage ($V_{Electrode}$) varying from -0.5 V to 1.5 V . Fig. 8(a) shows pH-induced transfer curves for a SiNR array ISFET made up of 15 wires, each measuring 50 nm width.

An increase of V_{TH} is achieved by increasing the pH level of the buffer solution (decreasing H^+ concentration). The change in surface charge density induced by a pH modification is described by the site-binding model [7] which

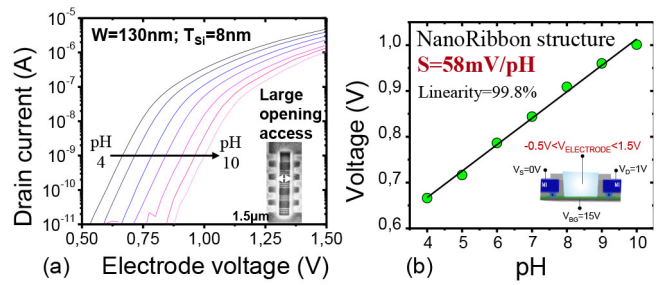


FIGURE 8. (a) pH sensitivity of a Si NR array-based pH sensor. (b) Electrode voltage vs pH solution varying from 4 to 10. A pH-response of 58 mV/pH is achieved, which is in good agreement with the Nernstian sensitivity of 59.5 mV/pH at 300 K .

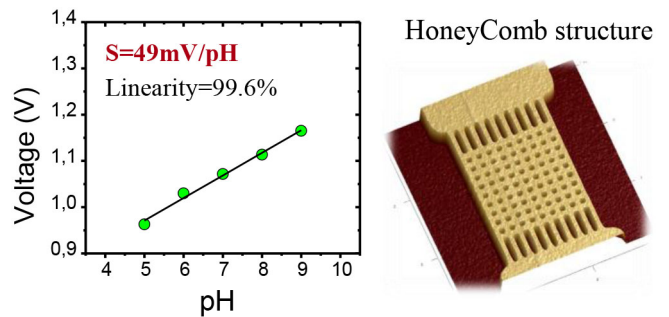


FIGURE 9. pH sensitivity of Si honeycomb-based pH sensors. A pH-response of 49 mV/pH is achieved.

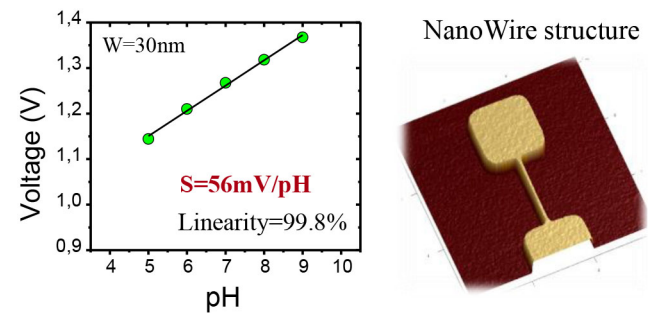
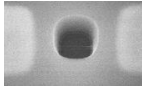

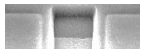

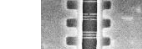



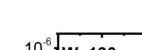
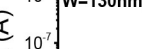
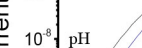




FIGURE 10. pH sensitivity of Si nanowire-based pH sensors. A pH-response of 56 mV/pH is achieved.

takes into account the protonation and deprotonation of OH groups lining the surface of HfO_2 dielectric. This model predicts an approximately linear relation between the gate oxide surface charge density and the pH of the electrolyte. In Fig. 8(b), this linear relationship is experimentally demonstrated with a slope of 58 mV/pH (extracted at $I_{DS} = 10^{-9}\text{ A}$) which is very close to the ideal Nernstian behavior at 300 K (59.5 mV/pH).

We assessed the pH sensitivity on different geometries of bioFET with the same measurement protocol. Once again, as shown in Fig. 9-10, a pH response of 49 mV/pH and 56 mV/pH are obtained for HC and NW structures respectively. The pH sensitivity related to the different geometries of bioFETs is summarized in Table 1. For all geometries studied, we obtained a nearly ideal Nernstian response between ~ 50 and 68 mV/pH . It should be noted that for

TABLE 1. Summary of pH sensitivity. No significant differences are observed between NW, NR or HC structures.

	Device ID	W (μm)	L (μm)	S (mV/pH)
	Single NW	0.05	0.4	68
	Single NW	0.05	0.45	68
	Single NW	0.05	0.5	68
	Single NW	0.05	0.3	56
	NR	0.5	10	64
	NR	1.07	1	60
	NR	1.07	5	60
	Array of NR	0.15 (x5)	1.5	58
	Array of NR	0.15 (x5)	1.5	62
	Array of NR	0.15 (x5)	1.5	63
	Array of NR	0.08 (x10)	5	66
	Honeycomb	0.05x0.05	1.05	49
	Honeycomb	0.05x0.05	2.05	60

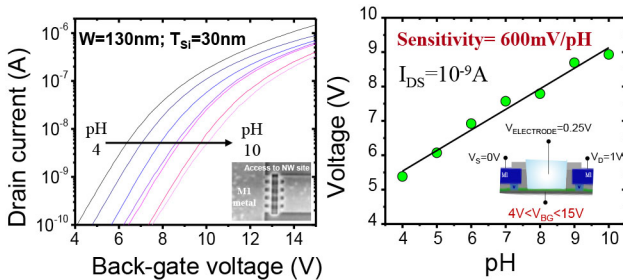


FIGURE 11. Transfer characteristics of Si NR array-based pH sensors with pH solutions varying from 4 to 10. The bias of our reference electrode is 0.25 V and $V_{DS} = 1$ V. The device exhibits a significantly enhanced pH sensitivity of 600 mV/pH due to the capacitive coupling between the reference electrode and the back-gate electrode.

access opening below 210 nm, no sensor devices are functional. This probably defined the limit of wettability inside small open cavities.

In a second step, we measured the pH-induced V_{TH} shift of NR structures at a fixed liquid potential ($V_{Electrode} = 0.25$ V) when sweeping the back-gate voltage (V_{BG}).

As shown in Fig. 11, in this operating mode, the sensitivity measured on the device greatly exceeds the Nernst limit to reach the value of 600 mV/pH. This enhancement of sensitivity is explained by a capacitive coupling between the reference and the back-gate electrodes. In the case of fully depleted devices, the interaction between both electrodes can be described by the following equation [12], [13]:

$$\Delta V_{TH}^{BG} = \frac{3 \times t_{BOX}}{(3 \times t_{OX} + t_{Si})} \Delta V_{TH}^{REF} \quad (1)$$

where t_{BOX} , t_{ox} , and t_{Si} represent respectively the buried-oxide thickness, the front-gate oxide, and the channel thickness. ΔV_{TH}^{BG} and ΔV_{TH}^{REF} are the threshold voltages related to the back-gate and reference electrode. This leads to an amplification factor of **9.5** which is well consistent with the enhancement of sensitivity ($\times 10$) induced by

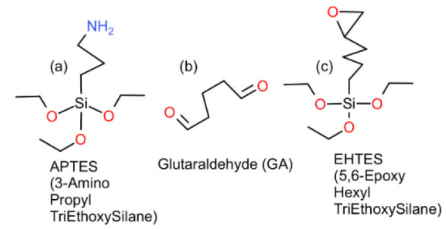


FIGURE 12. Molecules of (a) APTES, (b) GA, and (c) EHTES.

the capacitive coupling (Eq. (1)). These results are well consistent with the work published by Park *et al.* [12].

IV. BIOLOGICALLY SENSITIVE FETS

A. PROTOCOLS OF FUNCTIONALIZATION

The quality of the functionalization layer is of key importance in the development of selective, ultrasensitive and reliable biosensors [14]. Here, the surface functionalization consists of methods by which conjugation of a monolayer of probe molecules is made to the surface of the transducer of a biosensor (i.e., oligonucleotides, aptamers, etc. *versus* bioFET gate oxide or other transducers). Surface functionalization is a research area in its own right, and there are a large number of chemical techniques allowing for modification of surfaces [15]. Here, we have chosen to functionalize our gate oxides by silanization, a well-documented technique, easy to implement, and commonly used in academic and industrial laboratories [16]. Silanization process introduces an organosilane molecule that produces a self-assembled monolayer covalently bonded to the underlying substrate (i.e., oxides or other materials). The final role of this coating monolayer is to serve as an intermediate linker between the “substrate” and the “organic receptors” capable of specific interaction with the targeted species to be detected.

To graft our organic receptors, i.e., single strand DNA probes (ssDNA) on our HfO_2 gate oxide, we started the functionalization tests with the widespread “APTES” silanization protocol that uses a pair of coating molecules, namely “3-aminopropyl triethoxysilane” and “glutaraldehyde” (APTES/GA) Fig. 12(a), (b) as a crosslinker between the surface of the oxide and the DNA probes [16]–[18].

Before being widely used on our bioFETs gate oxide, we validated this protocol on planar SiO_2 surfaces. After APTES/GA covalent coating, ssDNA probes are grafted over these intermediate layers.

Hybridization assays made over the ssDNA probe grafted-sample with complementary or non-complementary fluorolabelled target DNA allow for optical characterization by fluorescence imaging. The characterization results obtained with this protocol led us to highlight non-idealities (non-specific adsorption events and heterogeneous coating) and therefore to segment the observed fluorescence into multicausal fluorescences arising from different interactions between the fluorolabelled target DNA and other reagents. To overcome these non-specific interactions, we

worked with a second silanization protocol, more robust and more efficient, in which we used an epoxysilane (“5,6-epoxyhexyltriethoxysilane”, EHTES) (Fig. 12(c)) to anchor the ssDNA probes directly on the EHTES-coated surface without additional crosslinker. These different protocols of functionalization used both on planar SiO₂ surface and HfO₂ gate oxide are presented and discussed in the following sections.

A.1. GAS PHASE SALINIZATION USING APTES/GA LINKERS

As a preliminary step towards the functionalization of our bioFETs HfO₂ gate oxide, APTES/GA molecules was used to conjugate covalently ssDNA probes on planar SiO₂ samples. We performed a thermal oxidation of bulk silicon (725 μm thick) to achieve a 93 nm thick SiO₂ oxide. This combination of thicknesses corresponds to an optimal dimensioning for which it has been shown that a maximal intensity of fluorescence signal can be collected during fluorescence imaging [19]. Then, we diced the substrate in individual samples of 10 mm × 10 nm size.

Sample cleaning procedure: The functionalization process starts with a cleaning step of the diced sample that consists in immersing it in a consecutive ultrasonic 10 min baths of acetone, ethanol, and deionized water. The objective is to remove the small particles and organic residues from the sample surface. After cleaning, the sample is blow-dried with an argon gas gun.

Hydroxylation: The surface hydroxylation step aims to create a saturated density of superficial hydroxyl groups (–OH) on the SiO₂ surface (namely silanol groups Si–OH), following the ionization reaction “Si–O–Si + energetic Air–H₂O plasma = Si–OH + Si–OH”. For this, we introduced the sample into an internal vacuum chamber of a plasma cleaner where an Air plasma discharge ionizes its surface during ~5 min (Evactron, set to 12 Watts, 4 × 10^{–1} Torr).

APTES silanisation: After superficial hydroxylation, we inserted and handled the sample into a low humidity (<1%) nitrogen-filled glove box. The sample is placed into a dry Teflon vial, near a small cup of ~150 μL aqueous APTES. The vial is sealed and baked at 80°C during one hour, during which the surface undergoes a gas phase silanization process. Evaporated and hydrolyzed molecules of APTES simultaneously form a film of “homo-condensed” APTES molecules that “hetero-condenses” itself at the locations of silanol sites [16], [18]. At this point, molecular interactions between homo and hetero condensed APTES are based on weak hydrogen bonds. The rinsing of the sample with absolute ethanol removes unreactive APTES molecules. After rinsing, the sample is blow-dried with a N₂ gas gun.

Annealing: After the gas-phase silanization process, the next step consists in another baking session at 110°C for three hours, during which residual traces of water molecules and hydrogen bonds are chemically dehydrated into covalent siloxane links (Si–O–Si) [16].

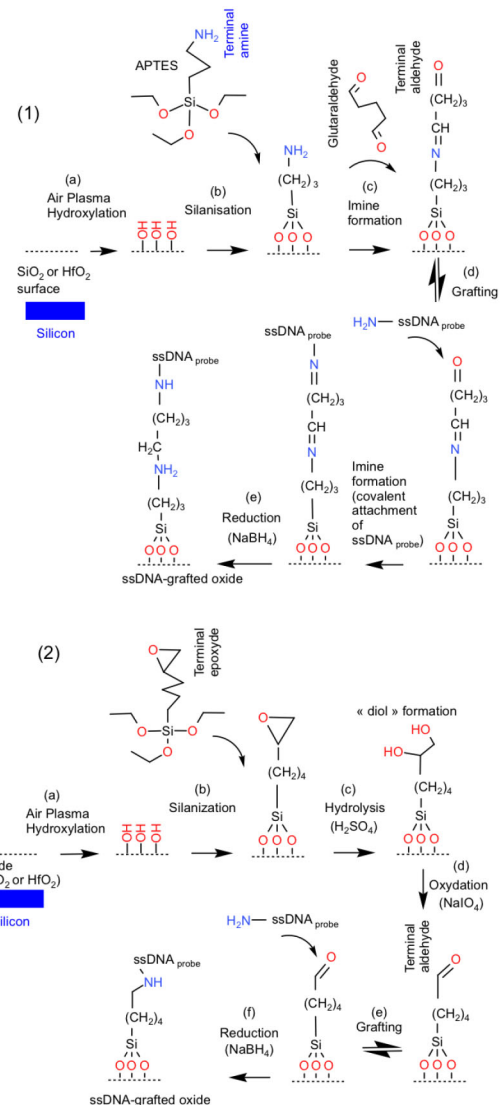


FIGURE 13. Oxide biofunctionalization with ssDNA probe through (1) “APTES/GA” functionalization protocol and (2) EHTES protocol.

Glutaraldehyde coating: Glutaraldehyde (GA, C₅H₈O₂) is a saturated dialdehyde commonly used as a cross-linker molecule to link two distinctive amine groups (NH₂) on either side of the molecule (Fig. 13.1(c), (d)). Here, the role of the GA layer is to serve as an anchoring layer for the upcoming NH₂-conjugated ssDNA probe molecules. This step consists in dipping the sample in a diluted by half GA solution during 1.5 hours at 300K. Spontaneous covalent imine formation occurs between the aldehyde functional groups of GA and the amine functional groups present at the APTES molecules extremities, thereby conjugating the GA layer to the APTES layer (Fig. 13.1(c)). After GA coating, the sample is thoroughly rinsed with deionized water and N₂ blow-dried.

Biomolecule immobilization (ssDNA probes grafting): The last step of functionalization consists in depositing droplets of 2 μL of variable concentrations of complementary or

TABLE 2. DNA sequences.

complementary ssDNA probe	non-complementary ssDNA probe	Cy3-target DNA
NH ₂ -(CH ₂) ₆ -GCA GCT	NH ₂ -(CH ₂) ₆ -AGT TGG	Cy3-GG CAG CCG
CAT CAC GCA GCT	GTG GTG AGT AGG	AAG GGC ATG AGC
CAT GCC CTT CGG	GTG AGG GGG GAA	TGC GTG ATG AGT
CTG CC	GGA GG	TGC

non-complementary ssDNA probes (concentration ranging between 0.1 and 200 μ M) on the APTES/GA-functionalized sample. The sequences of the DNA molecules are described in Table 2. The deposition is done with a manual micropipette without using a microspotting tool. After deposition of ssDNA probes, we inserted the sample into a high rate humidity crystallizer and left it to react during several hours (between 2 and 12 hours) for spontaneous self-grafting of NH₂-ssDNA probes over the GA layer, at the sites of free aldehydes, through imine formation. After this incubation step, we rinsed the ssDNA-grafted sample with deionized water and blow-dried it with a N₂ gas gun.

Chemical stabilization: In order to introduce more chemical stability in the overlaying conjugated layers, we immersed the sample into a solution of a reductive reagent (Sodium borohydride, NaBH₄) allowing for the reduction of the reactive double bonds (present on imines and aldehydes) into relatively chemically stable single bonds (amines and alcohols) (Fig. 13.1(e)). The sample is rinsed with deionized water, washed with Sodium Dodecyl Sulfate (SDS) and rinsed another time before drying and storage in a dry enclosure. The main steps of this protocol are depicted in the Fig. 13.1.

ssDNA probes/Cy3-target DNA hybridization: After grafting, we performed a DNA hybridization assay over the functionalized samples. A sufficient quantity of \sim 2 μ L of 2 μ M cyanine-3 fluorolabelled target DNA (Cy3-target DNA, Table 2) is deposited on each region where ssDNA probes were grafted. The target DNA solutions are spread over the entire surface of the sample with a HybriSlip Hybridization film and the complex is inserted in a high humidity (>80%) glass Petri dish. The hybridization reaction can be outlined in several phases. First, we inserted the sample in an oven during \sim 30 min at 75°C for the needs of DNA strands unfolding from folded structure to linear strand capable of hybridization. Secondly, we decreased the temperature to \sim 50°C for 30 min to give place to ssDNA probe/target DNA hybridization if the strands are complementary. Finally, the sample is taken out from the oven to cool under a fume hood for at least 15 min.

Post-hybridization washing: After the hybridization assay, we washed the sample with 2 \times and 0.2 \times decreasing concentration of saline-citrate solution (SSC, pH 7) during 2 min each, on an orbital shaker set at high speed. Then, we rinsed the samples with deionized water, blow-dried it with N₂ and stored it away from light. The purpose of this rinsing is to eliminate non-hybridized/non-fixed target DNA molecules.

The SSC salts have the role of fixing the free DNA molecules and thus causing their elution.

Surface characterization: Then, we characterized the sample surface with a fluorescence microscope Olympus BX41M connected to a Scion CFW-1308M digital camera. Cy3 dyes conjugated to the target DNA molecules allow for easy optical traceability of the target DNA interactions with the sample surface components (i.e., localization, interactions, bulk structures, etc.).

A.2. LIQUID PHASE SILANISATION USING EHTES LINKER

Here, the main differences with the APTES/GA gas phase silanisation rely on the silanisation process and the absence of GA coating treatment. All of the other process remain similar and valid for both protocols.

EHTES silanisation: After surface cleaning and hydroxylation, we immersed the samples into a sealed vial containing 0.12% EHTES silane and 3.4% triethylamine diluted in toluene, and baked it at 80°C for 16 hours. An annealing session is performed after silanisation for dehydration. The epoxy terminals of the EHTES are hydrolyzed into diols terminals during a chemical reaction where the sample is immersed into a 5% Sulfuric acid solution (H₂SO₄) for 2 hours. The next step is the formation of aldehyde terminals, made by immersing the sample into a solution of 0.1M Sodium periodate (NaIO₄). Diols undergo oxidation and product aldehydes, thus making the pool of NH₂-ssDNA probes anchorage possible on the EHTES layer, without any crosslinker or additional intermediary (Fig. 13.2). Then, we deposited microdroplets of \sim 300 pL of ssDNA probes on the sample surface by an ultra-low volume dispensing system (Scienion, Sciflexarrayer).

B. FUNCTIONALIZATION RESULTS AND DISCUSSION

B.1. METHODS OF CHARACTERIZATION

Contact angle measurement: One first way to check the effectiveness of the silanisation process is to run contact angle measurements on the silanized samples.

After hydroxylation, our samples exhibit low contact angle values of \sim 1° on average. This is consistent with the fact that produced hydroxyl radicals (-OH) constitute highly hydrophilic active sites, thus justifying the extremely low contact angle values. We evidenced the definitive bonding of the silane layer over the SiO₂ oxide surface by a significant increase of the contact angle of almost 45 \pm 10° due to APTES or EHTES layer relative hydrophobicity. These measurements show a successful silanisation of the oxidized surface.

Surface characterization by fluorescence: We performed surface characterization for different samples to confirm specific pairing of Cy3-target DNA with the grafted ssDNA probes. The Fig. 14 (2-4) presents typical micrographs resulting from a functionalized surface after DNA hybridization in the case of APTES/GA protocol. The results show that we successfully reproduced

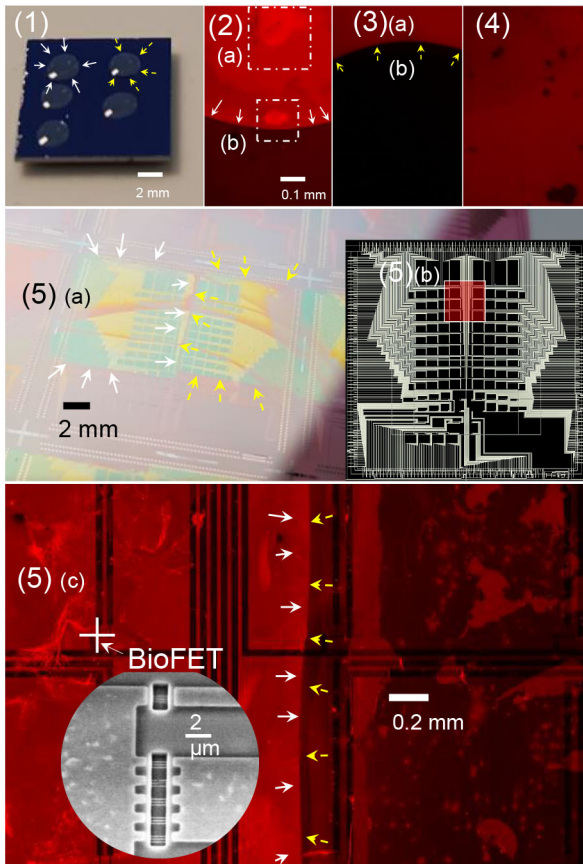


FIGURE 14. Fluorescence micrographs of different regions of interest showing attachment of Cy3 fluorolabelled target DNA molecules over the ssDNA probe-grafted substrate (thermal SiO₂ or HfO₂ gate oxide) in the case of APTES/GA protocol. (1) Photograph of a SiO₂ dice with deposited solution of ssDNA probes. White arrows surround complementary ssDNA probes droplet and yellow dashed arrows surround non-complementary negative control ssDNA probes. (2)(a) Hybridization of complementary Cy3 fluorolabelled target DNA. The white arrows show the borders of the pool of complementary ssDNA probes, coincident with the limits of the region of aggregation and hybridization of the target DNA molecules. The white squares show heterogeneous fluorescence. (2)(b), (3)(a) and (4) depict APTES/GA-functionalized background characterized by non-null fluorescence. (3)(b) Absence of fluorescence over the negative control region where a pool of non-complementary ssDNA probes is grafted. The yellow dashed arrows show the grafting delimitation, coincident with the limit of the region of zero fluorescence. (5)(a) "APTES/GA" functionalized biochip. (b) layout of a biochip showing the photographed region in the (5)(c) micrograph.

the APTES/GA functionalization protocol with our tools. As expected, oligonucleotide hybridization phenomenon is observed over the functionalized SiO₂ sample and this result has been reproduced several time before widely using the protocol for the grafting of bioFETs (Fig. 14.5 (c)).

B.2. NONSPECIFIC CY3-TARGET DNA INTERACTIONS

While it has been effective to graft ssDNA probes over oxidized surfaces, the APTES/GA functionalization protocol has shown imperfections such as inhomogeneity and background fluorescence. These non-idealities directly denote the limitation of this functionalization protocol. An optimal grafted layer should result in a reproducible and homogenous monolayer. Additional measurements (Fig. 15)

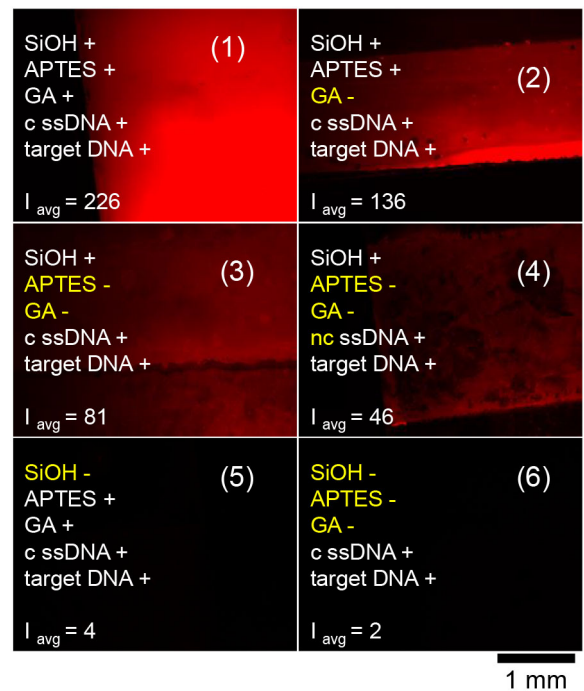


FIGURE 15. Micrographs of differently functionalized SiO₂ sample surface in the case of APTES/GA protocol. (1) Standard biofunctionalized sample showing Cy3-target DNA specifically localized over the complementary ssDNA probe-grafted region. (2) The absence of GA coating highlights APTES/Cy3-target DNA and or APTES/ssDNA probes nonspecific interactions. (3) and (4) Hydroxylated SiO₂ surface without APTES/GA (APTES- and GA-) showing Si-OH/DNA nonspecific interactions. (5) and (6) Non hydroxylated SiO₂ (SiOH-) surface showing near zero fluorescence. I_{avg} stands for average intensity of fluorescence on an 8-bit grayscale.

enabled us to justify these artifacts by nonspecific interactions including DNA/APTES interactions, physical adsorption (physisorption) of DNA over silanol groups, and potential bridging of APTES molecules by GA crosslinkers. GA-bridged APTES structures ((APTES-GA-APTES)_n) should hamper correct anchoring of ssDNA probes since GA aldehyde groups link amines of APTES instead of amines of NH₂-ssDNA probes. Increasing the concentration of GA to cover more free APTES sites resulted in a decrease of fluorescence signal. Our hypothesis is that the addition of a large amount of GA shifts the chemical equilibrium in favor of GA-bridged APTES production, thereby lowering NH₂-ssDNA anchoring and later Cy3-target DNA hybridization. DNA oligonucleotides being negatively charged, the non-specific interactions of APTES/DNA and silanol/DNA may be of electrostatic nature. We have deduced from these experiments that in the APTES/GA functionalization protocol, the resulting fluorescence is the combination of specific hybridization fluorescence (complementary ssDNA probes/target DNA) with nonspecific ones, as emphasized in Fig. 15.

B.3. EHTES FUNCTIONALIZATION RESULTS

To overcome the limitations of APTES/GA protocol, we used the EHTES silanization method. The results (Fig. 16)

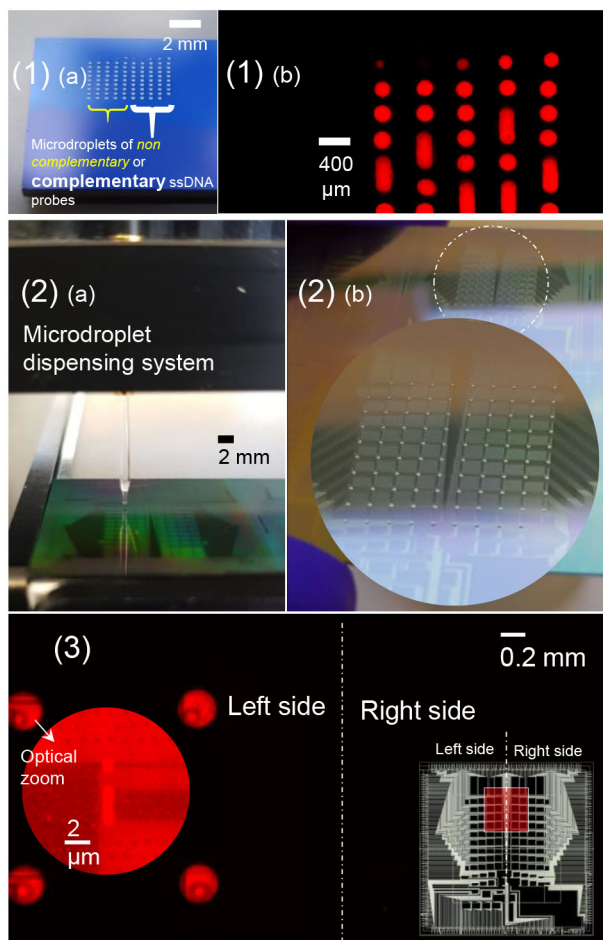


FIGURE 16. Micrographs of samples functionalized with EHTES protocol. (1)(a) Functionalized SiO_2/Si dice imaged just after the robot-assisted deposition of ssDNA probe microdroplets. (1)(b) Fluorescence micrograph of the same dice after Cy3 target DNA hybridization assay. (2)(a) Robot-assisted grafting of a biochip (2)(b) ssDNA probe-grafted biochips with visible microdroplets (3) Post hybridization assay fluorescence micrograph of a grafted biochip. ssDNA probes are complementary at the left side of the chip and non-complementary at the right side. Fluorescence spots are coincident with complementary ssDNA probes, confirming the effectiveness of the EHTES protocol.

showed significant improvements such as a more homogeneous visual appearance of the hybridized spots, a better level of background fluorescence noise, and the reproducibility of the repeated functionalization runs. Furthermore, the use of a microdroplet dispensing system facilitates the deposition of ssDNA probes in close proximity of the bioFET sensors. This also leads to the shrinkage of the area where ssDNA probes can pair with target DNA, and therefore decreases the loss of target DNA molecules of interest outside the sensing cavities of bioFETs.

B.4. DEPENDENCE ON DNA PROBE CONCENTRATION

An optimal density of grafted ssDNA probes over the sensing module (i.e., gate oxide) is essential to the formation of a homogeneous, dense and tangle-free monolayer, necessary for enhanced performance in detection of target

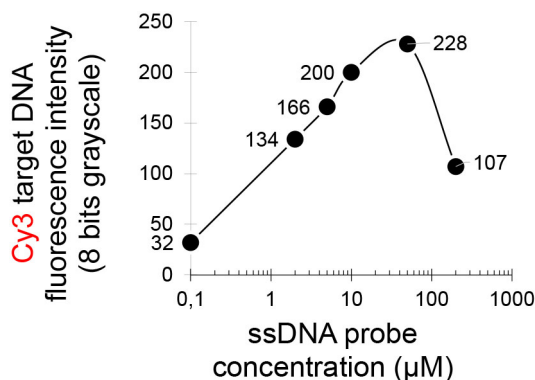


FIGURE 17. Effect of concentration of ssDNA probes on the hybridization efficiency.

DNA. Indeed, the target DNA oligonucleotides should be able to inlay easily before undergoing hybridization without steric hindrances impeding the hybridization process. Thus, our objective was to determine an efficient ratio of concentrations “grafted-ssDNA probes/target DNA” for which the hybridization condition is optimal. For this, we used planar thermal SiO_2/Si samples, functionalized by the APTES/GA protocol. Concentration of grafted ssDNA probes varies by the values of 0.1, 2, 5, 10, 50 and 200 μM , and the concentration of target DNA is kept fixed at 2 μM . The concentration of the ssDNA probes is the limiting concentration since for the same quantity of fluorescent target DNA, the fluorescence intensity will depend on the quantity of available ssDNA probes. The maximum of fluorescence was obtained in the configuration of 50 μM of ssDNA probes, suggesting an optimal hybridization ratio of 25 (Fig. 17). Beyond this ratio, the efficiency of hybridization decreases. This result is in good agreement with the ones reported by other groups[20]–[22].

C. CONCLUSION ON FUNCTIONALIZATION PROTOCOL

The use of standard silanization methodology involving APTES/GA intermediates allowed us to functionalize planar oxide surfaces as well as bioFET devices. We have shown that the phenomenon of hybridization occurs or not, in well accordance with the complementary or non-complementary nature of the covalently grafted ssDNA probes. However, this protocol entailed high-level of background fluorescence and randomly located inconsistencies over the fluorescence region. We justified these artifacts by non-specific electrostatic interactions between DNA oligonucleotides and both layers of silanol and APTES. By increasing GA concentration to coat more efficiently the APTES layer, we observed a decrease in the grafting efficiency that we explained by the formation of GA-bridged APTES structures that are inapt to anchor ssDNA probes. To overcome these limitations, we used the epoxysilane EHTES silanization method, which allows for direct grafting of ssDNA probes without

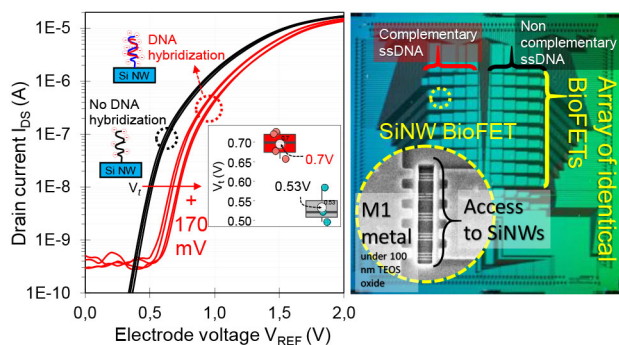


FIGURE 18. Electrical characterization of SiNW array sensors with hybridized 2 μM Cy3-target DNA molecules (red curves) versus non-complementary ssDNA probes-grafted control sensors (black curves). $V_{DS} = 1\text{ V}$ and $V_{BG} = 6\text{ V}$. V_{TH} values are extracted at $I_{DS} = 10^{-8}\text{ A}$.

cross-linkage agent. Finally, we shown that a probe to target concentration ratio of 25 is an ideal value to optimize DNA hybridization.

V. ELECTRICAL DETECTION OF DNA HYBRIDIZATION

In the last step, after DNA grafting, we electrically detected the DNA hybridization. Therefore, we first deposited an electrolyte solution of pH 7 above each sensor for DNA resuspension. As shown in Fig. 18, hybridization of Cy3-target DNA induces a significant V_{TH} shift (+170 mV) of I_{DS} - $V_{Electrode}$ curves, which is well consistent with the contributive effect of supernumerary negative charges carried by the target DNA strands. Similar outcomes have been replicated in 4 other different biochips among which two were grafted with 14 oligonucleotides length ssDNA probes to detect 14 nucleotides length Cy3-target DNA. Systematic biosensing measurements at wafer-scale level to investigate variability as well as temporal drift of output characteristics will shortly be performed.

VI. CONCLUSION

In this work, we fabricated a CMOS compatible bioFET for pH sensing and label-free DNA hybridization detection. Dual gate operation mode has led us to reach a super Nernstian sensitivity of $\sim 600\text{ mV/pH}$. In a second step, we deeply investigated two different protocols of functionalization. Due to the observation of nonspecific interactions occurring with APTES/GA functionalization protocol, we assessed and used EHTES epoxysilane functionalization protocol, which is better suited for the fabrication of a high quality covalently grafted ssDNA probe layer. Finally, after running hybridization assays with 2 μM target DNA, the tested SiNW array devices showed a significant increase of V_{TH} (+0.17V) in comparison with the non-complementary ssDNA grafted control devices. Given its compatibility with conventional CMOS processing technology, this bioFET should have wide applicability for chemical and biomedical sensors.

REFERENCES

[1] J. M. Rothberg *et al.*, "An integrated semiconductor device enabling non-optical genome sequencing," *Nature*, vol. 475, no. 7356, pp. 348–352, 2011, doi: [10.1038/nature10242](https://doi.org/10.1038/nature10242).

[2] B. R. Dorvel *et al.*, "Silicon nanowires with high-k hafnium oxide dielectrics for sensitive detection of small nucleic acid oligomers," *ACS Nano*, vol. 6, no. 7, pp. 6150–6164, 2012, doi: [10.1021/nn301495k](https://doi.org/10.1021/nn301495k).

[3] G. Zheng, F. Patolsky, Y. Cui, W. U. Wang, and C. M. Lieber, "Multiplexed electrical detection of cancer markers with nanowire sensor arrays," *Nat. Biotechnol.*, vol. 23, no. 10, pp. 1294–1301, 2005, doi: [10.1038/nbt1138](https://doi.org/10.1038/nbt1138).

[4] A. Poghosian, M. Jablonski, D. Molinnus, C. Wege, and M. J. Schöning, "Field-effect sensors for virus detection: From ebola to SARS-CoV-2 and plant viral enhancers," *Front. Plant Sci.*, vol. 24, Nov. 2020, Art. no. 598103, doi: [10.3389/fpls.2020.598103](https://doi.org/10.3389/fpls.2020.598103).

[5] N. Shehata *et al.*, "Silicon nanowire sensors enable diagnosis of patients via exhaled breath," *ACS Nano*, vol. 10, no. 7, pp. 7047–7057, 2016, doi: [10.1021/acsnano.6b03127](https://doi.org/10.1021/acsnano.6b03127).

[6] P. Bergveld, "Thirty years of ISFETOLOGY: What happened in the past 30 years and what may happen in the next 30 years," *Sensors Actuators, B Chem.*, vol. 88, no. 1, pp. 1–20, Jan. 2003, doi: [10.1016/S0925-4005\(02\)00301-5](https://doi.org/10.1016/S0925-4005(02)00301-5).

[7] D. E. Yates, S. Levine, and T. W. Healy, "Site-binding model of the electrical double layer at the oxide/water interface," *J. Chem. Soc. Faraday Trans. 1 Phys. Chem. Condens. Phases*, vol. 70, no. 10, p. 1807, 1974, doi: [10.1039/f19747001807](https://doi.org/10.1039/f19747001807).

[8] D. Nozaki, J. Kunstmann, F. Zörgiebel, and G. Cuniberti, "Influence of surface charge on the transport characteristics of nanowire-field effect transistors in liquid environments," *Appl. Phys. Lett.*, vol. 106, no. 20, 2015, Art. no. 203104, doi: [10.1063/1.4921401](https://doi.org/10.1063/1.4921401).

[9] L. Mu, Y. Chang, S. D. Sawtelle, M. Wipf, X. Duan, and M. A. Reed, "Silicon nanowire field-effect transistors—A versatile class of potentiometric nanobiosensors," *IEEE Access*, vol. 3, pp. 287–302, 2015, doi: [10.1109/ACCESS.2015.2422842](https://doi.org/10.1109/ACCESS.2015.2422842).

[10] N. Elfström, R. Juhasz, I. Sychugov, T. Engfeldt, A. E. Karlström, and J. Linnros, "Surface charge sensitivity of silicon nanowires: Size dependence," *Nano Lett.*, vol. 7, no. 9, pp. 2608–2612, 2007, doi: [10.1021/nl0709017](https://doi.org/10.1021/nl0709017).

[11] S. Zafar, C. D'Emic, A. Afzali, B. Fletcher, Y. Zhu, and T. Ning, "Optimization of pH sensing using silicon nanowire field effect transistors with HfO₂ as the sensing surface," *Nanotechnology*, vol. 22, no. 40, 2011, Art. no. 405501, doi: [10.1088/0957-4484/22/40/405501](https://doi.org/10.1088/0957-4484/22/40/405501).

[12] J.-K. Park, H.-J. Jang, J.-T. Park, and W.-J. Cho, "SOI dual-gate ISFET with variable oxide capacitance and channel thickness," *Solid. State. Electron.*, vol. 97, pp. 2–7, Jul. 2014, doi: [10.1016/j.sse.2014.04.036](https://doi.org/10.1016/j.sse.2014.04.036).

[13] H.-J. Jang and W.-J. Cho, "Performance enhancement of capacitive-coupling dual-gate ion-sensitive field-effect transistor in ultra-thin-body," *Sci. Rep.*, vol. 4, p. 5284, Jun. 2014, doi: [10.1038/srep05284](https://doi.org/10.1038/srep05284).

[14] E. L. Sciuto *et al.*, "Functionalization of bulk SiO₂ surface with biomolecules for sensing applications: Structural and functional characterizations," *Chemosensors*, vol. 6, no. 4, p. 59, 2018, doi: [10.3390/chemosensors6040059](https://doi.org/10.3390/chemosensors6040059).

[15] J. J. Gooding and S. Ciampi, "The molecular level modification of surfaces: From self-assembled monolayers to complex molecular assemblies," *Chem. Soc. Rev.*, vol. 40, pp. 2704–2718, Feb. 2011, doi: [10.1039/c0cs00139b](https://doi.org/10.1039/c0cs00139b).

[16] M. Zhu, M. Z. Lerum, and W. Chen, "How to prepare reproducible, homogeneous, and hydrolytically stable aminosilane-derived layers on silica," *Langmuir*, vol. 28, no. 1, pp. 416–423, 2012, doi: [10.1021/la203638g](https://doi.org/10.1021/la203638g).

[17] R. G. Acres *et al.*, "Molecular structure of 3-aminopropyltriethoxysilane layers formed on silanol-terminated silicon surfaces," *J. Phys. Chem. C*, vol. 116, no. 10, pp. 6289–6297, 2012, doi: [10.1021/jp212056s](https://doi.org/10.1021/jp212056s).

[18] J. A. Howarter and J. P. Youngblood, "Optimization of silica silanization by 3-aminopropyltriethoxysilane," *Langmuir*, vol. 22, no. 26, pp. 11142–11147, 2006, doi: [10.1021/la061240g](https://doi.org/10.1021/la061240g).

[19] M. Bras *et al.*, "Optimisation of a silicon/silicon dioxide substrate for a fluorescence DNA microarray," *Biosens. Bioelectron.*, vol. 20, no. 4, pp. 797–806, 2004, doi: [10.1016/j.bios.2004.03.018](https://doi.org/10.1016/j.bios.2004.03.018).

[20] N. Zammattéo *et al.*, "Comparison between different strategies of covalent attachment of DNA to glass surfaces to build DNA microarrays," *Anal. Biochem.*, vol. 280, no. 1, pp. 143–150, 2000, doi: [10.1006/abio.2000.4515](https://doi.org/10.1006/abio.2000.4515).

[21] A. Gao *et al.*, "Enhanced sensing of nucleic acids with silicon nanowire field effect transistor biosensors," *Nano Lett.*, vol. 12, no. 10, pp. 5262–5268, 2012, doi: [10.1021/nl302476h](https://doi.org/10.1021/nl302476h).

[22] A. W. Peterson, R. J. Heaton, and R. M. Georgiadis, "The effect of surface probe density on DNA hybridization," *Nucleic Acids Res.*, vol. 29, no. 24, pp. 5163–5168, 2001, doi: [10.1093/nar/29.24.5163](https://doi.org/10.1093/nar/29.24.5163).